Composite Structures 311 (2023) 116794

Contents lists available at ScienceDirect

Composite Structures

journal homepage: www.elsevier.com/locate/compstruct

Performance enhancement of a bioinspired micro air vehicle by integrating a smart composite in its morphing wing

Javier Crespo Moreno [a], Rafael Bardera Mora [b], Ángel Antonio Rodríguez Sevillano [a], Álvaro Cobo González [a,*]

[a] Escuela Técnica Superior de Ingeniería Aeronáutica y del Espacio, Universidad Politécnica de Madrid, Plaza del Cardenal Cisneros, 3, 28040 Madrid, Spain
[b] Instituto Nacional de Técnica Aeroespacial (INTA), Carretera de Torrejón de Ardoz a Ajalvir, km 4,500, 28850 Torrejón de Ardoz, Madrid, Spain

ARTICLE INFO

Keywords:
Macro fiber composite
Piezoelectric
Micro air vehicle
Morphing
Finite element method

ABSTRACT

The purpose of this paper is to show the advantages of using a smart composite in a micro air vehicle (MAV) equipped with morphing wing technology. A Macro Fiber Composite (MFC) actuator is attached to the wing's bottom surface to modify the wing camber during the mission. This material allows the MAV to be optimized according to each flight, thus making it more versatile and attractive to the market. The elongation of the lower surface when a positive voltage is applied to the actuator is translated to an increment in camber, which results in an increment in the maximum lift coefficient, thus enabling the vehicle to fly slower to adapt to any payload. Besides, a reduction in camber results in an increase in aerodynamic efficiency, which improves range and endurance. Several tests of the MAV at prototype level have been carried out at INTA, so as to demonstrate the feasibility of implementing MFC actuators to control and manoeuvre these vehicles. The use of this material in aerospace industry opens up various fields of research in aerospace engineering, such as new features in flight mechanics and aerodynamic performance and new strategies in the design of flight stability and control laws.

1. Introduction

Ever since Leonardo da Vinci designed his famous ornithopter in the late 15th century after having thoroughly studied birds flight, aviation pioneers have undoubtedly found an endless source of inspiration in animal flight. However, the need for human-sized aircraft, capable of flying at a higher speed than birds and of lifting heavy payloads, has proven to be an important limitation in applying biological flight mechanics to human-made aircraft.

Nevertheless, recent technology development has led to the possibility to design air vehicles whose control orders originate either from an external pilot or from the vehicle itself, in the case of autonomous vehicles. Therefore, low-cost bird-sized micro air vehicles (MAVs) are now a feasible project [1], and the similarity between birds and MAVs' flight regime is a new possibility to adapt birds' flight mechanisms to aviation.

One of these opportunities is the development of morphing wings, i.e. wings whose features vary during flight in order to adapt to different flight conditions. In these terms, state-of-the-art smart composite materials are an outstanding choice to manage these geometry modifications, as their use allows a continuous deformation, more similar to that of the birds' wings, as well as a reduction in heavy control surfaces deflection systems. The purpose of this paper is to study and test the advantages of using a smart composite in a bioinspired autonomous MAV, the main objective being the optimization of the MAV's performance according to each mission, thus making the vehicle more versatile and attractive to the market.

This work is focused on the implementation of a macro-fiber composite (MFC) actuator attached to the wing's bottom surface in order to modify the wing's camber during the mission. This composite material, patented by NASA [2], uses d_{33} piezoelectric effect, which can produce a maximum fiber direction strain of 2000 μm/m when a 1500 V voltage is applied [3].

In this paper, a brief review of the morphing wing concept is carried out, followed by a concise overview of the elongation mechanism and features of the MFC. More importantly, the experimental tests and numerical simulations that have been conducted are then discussed, and their results are analyzed. Finally, the main conclusions are stated.

* Corresponding author.
E-mail addresses: javier.crespo@upm.es (J. Crespo Moreno), barderar@inta.es (R. Bardera Mora), angel.rodriguez.sevillano@upm.es (Á.A. Rodríguez Sevillano), alvaro.cobo.gonzalez@alumnos.upm.es (Á. Cobo González).

https://doi.org/10.1016/j.compstruct.2023.116794
Received 11 August 2021; Received in revised form 21 April 2022; Accepted 11 February 2023
Available online 16 February 2023
0263-8223/© 2024 The Authors. Published by Elsevier Ltd. This is an open access article under the CC BY license (http://creativecommons.org/licenses/by/4.0/).

2. Wing morphing

As stated above, wing morphing consists on the in-flight manipulation of the wing's external surface so as to improve aircraft performance by adapting aerodynamic features to each flight segment [4–7]. It is important to note that, in order to be considered as wing morphing, mechanisms have to manage a continuous shape deformation, which means traditional hinged control surfaces are excluded from this category. A widespread classification of morphing wing designs was proposed by Sofla et al. [4], who distinguished between in-plane morphing, out-of-plane morphing, and airfoil adaptation.

In-plane morphing mainly consists on the variation of wing area by altering its chord, sweep or span [5]. Out-of-plane morphing implies withdrawing the wing from its original plane, either by twisting or bending. This solution was already explored by the Wright brothers for their pioneer glider, whose coupled yaw-and-roll control system was based on this technique [6,7]. Finally, the main feature of airfoil adaptation designs is airfoil change with insignificant chord variation [8,9].

This paper focuses on a particular mechanism of out-of-plane transformation, which is on-flight camber alteration. This can be achieved reconfiguring the wing inner structure (ribs and spars, for instance) or inducing a deformation on the wing skin [4]. As the following paragraphs will explain, the studied prototype manages camber variation using MFC actuators that work on the wing skin. The desired consequences of implementing this technology are listed below.

First, an increment in camber would equal to an increment in the maximum lift coefficient, thus enabling the vehicle to fly with a lower speed and to record steadier and higher-quality videos or enhance its sensing accuracy. Moreover, high-camber configuration would be optimal for takeoff and landing maneuvers. On the other hand, a reduction in camber would result in an increase in aerodynamic efficiency, which would improve the range and endurance of the vehicle. Therefore, the resulting aircraft would be more versatile, being able to perform a wider range of missions, which would make it more appealing for potential customers. Furthermore, the use of MFC instead of classical mechanical systems produces a continuous deformation, which would enhance overall performance. Besides, it occupies less volume, which could be used for carrying more payload, and it weighs less, resulting in higher power-to-weight, lift-to-weight and lift-to-drag ratio.

The authors have performed an in-depth analysis of the aforementioned advantages, both through theoretical and wind tunnel studies. Research on the aerodynamics of the resultant MAV has successfully verified the expected performance enhancement effects. A detailed discussion of these studies can be found in [10,11].

3. Smart materials selected for wing morphing

Most wing morphing efforts are based on the implementation of smart materials that enable a deformation, extension or rotation of the wing surface or parts of it. These materials can produce a modification in the geometry of the wing without incurring in additional weight and costs that had previously hindered the profitability, and therefore the further development, of this technology [12]. Among smart materials, piezoelectric actuators (PZT), shape memory alloy actuators (SMA) and shape memory polymers (SMP) are the most frequent options for managing wing morphing [4].

Even though PZTs produce significantly lower strain output than SMAs, PZTs have higher actuation frequencies [13], which is desirable in the design of MAVs so as to achieve quicker responses. Besides, early attempts to use piezoelectric actuators in airfoil camber variation encountered two major obstacles: first, their brittleness limited their use, since handling and setting-up processes could cause breakage of the actuator, and second, the strain obtained with PZT stacks was insufficient to produce enough airfoil deformation to control an MAV [14]. Moreover, the use of lead-based PZTs entailed an undesirable weight penalization, and monolithic piezoceramic sheets had difficulty adapting to curved surfaces. This motivated the development of PZT composites, that combine voltage-induced actuation properties characteristic of PZTs and the ductility of the polymeric matrix [15]. Several additional benefits of this configuration can be mentioned. For instance, the flexibility of the matrix ensures a more precise adaptation to curved surfaces and the thickness of the fibers can be reduced. Additionally, the implementation of interdigitated electrodes can enhance the response of the material to a given applied voltage as the main piezoelectric effect (d_{33}) is strengthened, thus overcoming the second obstacle previously mentioned [16]. Therefore, a significantly higher in-plane actuation capability in relation to previous PZT through-the-thickness poling actuators is achieved.

An earlier counterpart of the MFC is the Active Fiber Composite (AFC). This material is made of cylindrical piezoceramic fibers that are uniaxially oriented within a polymer matrix and situated between two layers of interdigitated electrodes [17]. The application of a DC electric voltage between the aforementioned electrode layers provokes a positive strain in the fibers' direction. Moreover, AFCs also experience the opposite effect: the production of an electric stimulus as a result of a given strain. Therefore, it has been used both as an actuator and as a sensor [18] in many areas, e.g., structural health monitoring [19], vibration [20] and energy harvesting [21].

4. Macro Fiber Composite (MFC)

Notwithstanding, AFCs showed an important performance limitation, as the contact surface between the cylindrical fibers and the electrodes was insufficient. Besides, the fiber extraction process was manual and delicate, incurring in high costs [16]. This motivated the development of a new piezoceramic composite: MFC. As shown in Fig. 1, MFC has three different components: a layer of aligned piezoceramic rods with a rectangular cross-section, whose flexibility and damage tolerance are enhanced with respect to monolithic piezoceramic wafers; structural epoxy, which bonds fibers and electrodes and reduces fracture propagation in the fibers; and two polyimide films with interdigitated electrodes attached to them, which allow piezoelectric effects to take place [22].

The rectangular nature of the employed fibers entails a wider contact surface, whereas the fibers are obtained by dicing a low-cost piezoceramic wafer, thus overcoming the aforementioned disadvantages of AFCs. Moreover, an analytical study performed in [23] states the response of an MFC actuator is increased threefold with respect to an AFC actuator.

Actuators based on two piezoelectric effects are manufactured by Smart Material Corp. [22]. Their operation mechanisms are schematized in Fig. 2. Actuators using d_{31} effect work as contractors when voltages from −60 to 360 V are applied, and they require through-the-thickness poling. On the contrary, in d_{33} actuators, poling is performed in the direction of the fibers. This effect consists in an elongation of up to 1800 ppm when a voltage of 1500 V is applied, being −500 to 1500 V the range of applicable voltages [24]. However, strains higher than 1100 ppm have been found to cause fiber damage [16].

Both numerical and experimental studies have previously been conducted by several researchers in order to characterize MFC actuators' properties. First, Williams et al. conducted intensive research on the mechanical properties of this material, both in linear and non-linear range. The values obtained applying Classical Lamination Theory [25,26] were later experimentally verified [16]. Values provided by the manufacturer are situated between the results of both approaches followed by Williams et al., as shown in Table 1. Research carried out by Park et al. [23] led to a Classical Lamination Theory analysis whose results are practically equal to those obtained by Williams et al. Additionally, this paper predicts the properties of a single crystal MFC actuator, which is expected to have a 2.5 times higher actuation capacity. A numerical approach published by Deraemaeker et al. [31–33] focused on the properties of the active layer in the actuator. Its results

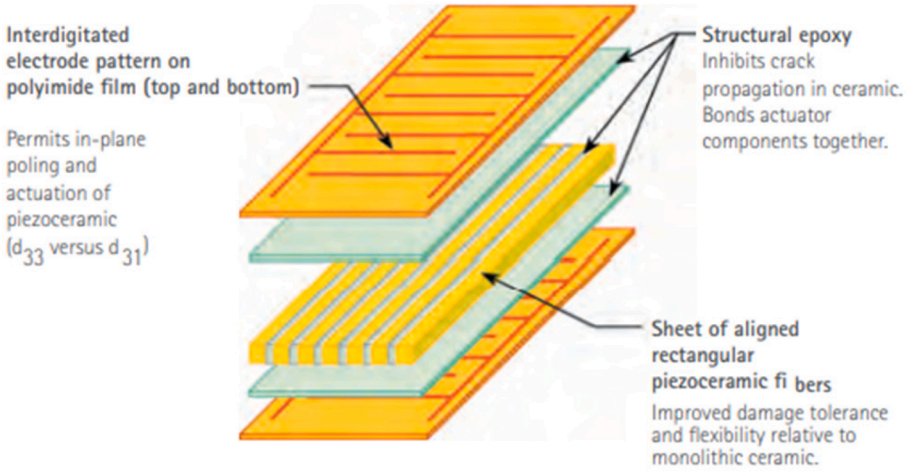


Fig. 1. Structure of an MFC actuator [22].

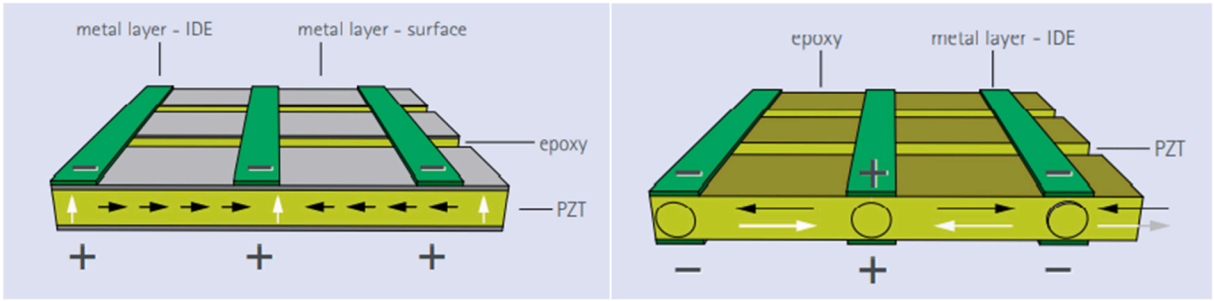


Fig. 2. Schematic operation process of d_{31} (left) and d_{33} (right) piezoelectric effects [22].

Table 1
Comparative values of MFC engineering properties.

	E_1 (GPa)	E_2 (GPa)	ν_{12}	G_{12} (GPa)
Reference values (Smart Material Corp.) [26]	30.34	15.86	0.31	5.52
Williams et al. (Classical Lamination Theory) [30]	31.2	17.1	0.30	5.27
Williams (Experimental results) [20]	29.4	15.2	0.31	6.06
Park et al. [27]	31.20	17.05	0.30	5.12
Deraemaeker et al. [33]	27.27	14.76	0.32	4.13
Biscani et al. [34]	32.95	16.03	0.35	–

were found to be compatible with Williams' experimental studies, even though they differed from the theoretical ones. Moreover, Biscani et al. [27] used an asymptotic expansion approach to compute these properties. Later works using numerical models to analyze the response of MFC integrated structures, such as composite plates and beams, [28,35–39] have predominantly taken both the values provided by Smart Material Corp. and by the early experimental studies by Williams et al. as a reference.

The mechanical behavior of an orthotropic material can be characterized with nine independent constants. Nevertheless, as MFC actuators are considered thin plates, this number can be reduced to four. Therefore, the results of the aforementioned studies are compared in Table 1. It can be inferred from Table 1 that Park et al. and Williams et al. theoretical results are very similar and are both near to the reference values. However, Deraemaeker et al. and Biscani et al. obtained, via numerical analysis, values that had a more important deviation from the experimental tests.

Consequently, considering the application analyzed in the present paper, the use of a d_{33} effect MFC plate firmly attached to the inside of the lower wing surface produces an elongation of the aforementioned surface when voltage is applied. As a result of the boundary conditions in the trailing and leading edge, the elongation of the lower surface is translated to an increment in camber, with a negligible variation in chord.

5. Experimental tests

As discussed above, MFC response to a given voltage is known. However, the deformation of a complex bioinspired wing design with embedded MFC actuators cannot be easily inferred from the values presented in Table 1. As a result, in order to study the effects of embedding MFC actuators in the structure of an MAV, and verify the aforementioned expected advantages, a bioinspired MAV has been designed. The main features of the studied aircraft are collected in Table 2.

The resulting prototype is shown in Fig. 3. A Zimmerman planform was chosen due to the need for a Low Aspect Ratio wing, derived from the strict dimension constraints and low typical Reynolds numbers that

Table 2
MAV prototype design features.

Wing planform	Zimmerman
Wing airfoil	Eppler E61
Wingspan (b) (m)	0.32
Wing area (S) (m^2)	0.041
Mean geometric chord (mgc) (m)	0.141
Mean aerodynamic chord (mac) (m)	0.170
Chord at wing root (c_r) (m)	0.20
Dihedral angle (Γ) (°)	10
Aspect ratio (AR)	2.5



Fig. 3. MAV prototype model.

characterize MAVs [28]. Within this context, Zimmerman wings provide an exceptional lift-to-drag ratio, only outperformed by well-studied elliptical wings [29]. Moreover, the selection of an E61 airfoil was motivated by its concave lower surface (Fig. 4), which is required to obtain a continuous variation in camber with the MFC actuator. Besides, performance at low Reynolds numbers has to be regarded. At first glance, an early development of a turbulent boundary layer is to be avoided because of the increment in skin friction drag it entails. However, the early detachment of the laminar boundary layer typical of E61 airfoil reduces the stall unpredictability found in flight at low Reynolds numbers. Additionally, stall is believed to be slightly delayed by this turbulent behavior. Further consideration on the prototype design features can be found in [11].

With the aim to study the deformation mechanism of the designed wing when attaching an MFC actuator to the internal side of its lower surface, a detached model of the half wing has been manufactured. The model has been cured in polyurethane molds produced via a computer numerical control (CNC) milling machine, which directly extracts the desired geometry from the 3D design developed using CATIA V5. This manufacturing process has been chosen because of its high reproducibility, its improved surface finish and its easiness to reproduce complex geometries. All this, beside the reduced production time, clearly counterbalances the required higher initial investment. Moreover, vacuum bags have been used to improve the curing process, as they offer reduced production time, better adaptation to the mold surface and an optimized fiber-to-resin ratio.

The 2 mm thickness model has been manufactured using standard fabric carbon fiber with a 200 g/m^2 density and epoxy L resin with EPH 161 catalyzer. The main properties of both components are summarized in Table 3, and the properties of the resultant composite material are collected in Table 4. Tables 3 and 4 include as well the characteristics of S-2 glass fiber and a composite material made up of these fibers and the aforementioned resin, which will be studied in next section.

An M-8528-P1 actuator manufactured by Smart Material Corp. [22] has been used. It was centered at 40 percent of the chord, so maximum camber point, which was originally situated at 51 percent of the chord, moves towards the leading edge when a positive voltage is applied.

Applied voltage has been progressively modified between −500 and 1500 V, corresponding to the operational limits stated by the manufacturer [22]. In order to do so, a 12 V DC power source has been attached to the power supply board, and the applied voltage has been varied using a control pin with voltages from 0 to 5 V. In Fig. 5, three different geometries are shown. The top image shows the resulting geometry for −500 V, the picture in the middle corresponds to 0 V, and the bottom image, to 1500 V. The expected increment in camber resulting from an increase in voltage can be observed. Therefore, these results validate the use of these technology for the performance enhancement

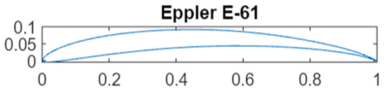


Fig. 4. Eppler E61 airfoil.

Table 3
Main properties of the composite material components.

	Epoxy L resin with EPH 161 catalyzer	Fiber Carbon/ Glass
Elastic modulus (E) (GPa)	3.4	238/88
Tensile strength (σ_u) (MPa)	70.2	3950/4500
Elongation at break (ε) (%)	9.5	1.7/5.6
Density (ρ) (g/cm^3)	1.158	1.76/2.47

Table 4
Main properties of the resultant composite material.

	Composite material Carbon/Glass		
Elastic modulus (E) (GPa)	70/25 (E_{11})	70/25 (E_{22})	4.5/4.0 (E_{33})
Shear modulus (G) (GPa)	5/5 (G_{12})	1.6/1.6 (G_{13})	1.6/1.6 (G_{23})
Poisson's ratio (ν)	0.1/0.2 (ν_{12})	0.1/0.2 (ν_{13})	0.1/0.2 (ν_{23})
In-plane tensile strength (σ_u) (MPa)	600/440		
In-plane compressive strength (σ_c) (MPa)	570/425		
In-plane shear strength (τ_{12}) (MPa)	90/40		
Density (ρ) (g/cm^3)	1.6/1.9		

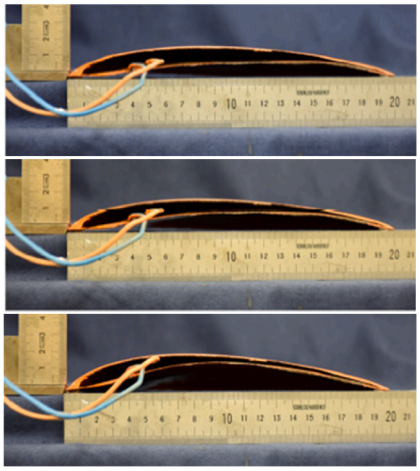


Fig. 5. Root airfoil geometries corresponding to −500 V, 0 V and 1500 V, respectively, from top to bottom.

purposes sought. Moreover, whereas the increment in camber is considerable, variations in chord are negligible, which is considered to be beneficial, as it will be easier to design a wing-fuselage joint.

Fig. 6 shows the Eppler E61 airfoil overlaid on the 0 V image, which corresponds to the unmodified geometry of the wing root cross-section. The picture displays the high accuracy achieved in the manufactured

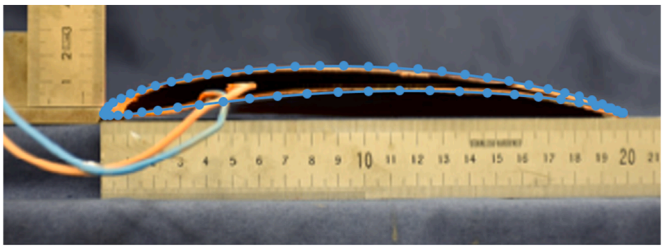


Fig. 6. E61 airfoil overlaid on the unmodified geometry of the prototype (0 V).

prototype.

Finally, the experimental points for maximum camber divided by the chord (dimensionless maximum camber: $\frac{f_{max}}{c}$) at the root versus output voltage (V) are collected in Fig. 7. Fig. 8 shows the definition of camber ($f(x)$), maximum camber (f_{max}) and chord (c).

A linear behavior can be inferred at first glance. Consequently, a linear fitting curve has been obtained:

$$\frac{f_{max}}{c}(\%) = 1.63 \bullet 10^{-3} \bullet V + 7.36$$

This function has a Pearson correlation coefficient of determination of 0.9773, indicating a very precise adjustment between experimental data and fitting curve.

6. Finite element method analysis

Even though analytical tests provide accurate results with respect to the behavior of the aircraft, it is not viable to manufacture a sufficient number of configurations so as to analyze the influence of varying different parameters. Besides, another advantage of using a finite element method (FEM) is that it allows to analyze deformation in all sections along the wingspan, whereas the experimental analysis was restricted to the section situated at the root. In order to perform an in-depth study of the effect of changing the materials and the layout of actuators, a finite element analysis using SOLIDWORKS® has been performed. As well as the carbon fiber composite defined in the previous section, an S-2 glass fiber composite made up of 110 g/m^2 density fibers and the same resin has been studied. The features of the fibers and the resulting composite are included in Tables 3 and 4, respectively. Both materials have been considered orthotropic. The state of maximum deformation, corresponding to an applied voltage of 1500 V has been studied.

FEM analysis was carried out employing a blended curvature-based mesh and a non-linear solver. This decision was motivated by the large displacements of both surfaces of the airfoil. Table 5 shows the main properties of this analysis.

Four different MFC layout configurations have been analyzed (Fig. 9). The actuators are depicted as a blue rectangle overlaid on the half-wing plan. Cases a, b and c have been studied with the aim to produce an increment in camber. It can be observed that variations in the position, size and number of actuators have been considered. Case d has been studied with the aim to increase the dihedral angle, since preliminary studies of the aircraft stability indicate that it has a positive dihedral effect, which affects stability negatively. This objective is achieved by positioning the actuators spanwise.

Resulting airfoils at position y = 20 mm for layout a and both carbon and glass fiber materials are shown in Fig. 10, which includes the original E61 airfoil as a reference.

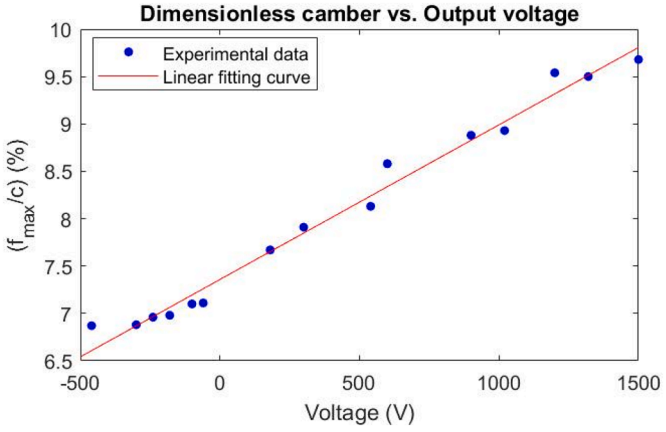


Fig. 7. Experimental data for dimensionless camber versus output voltage.

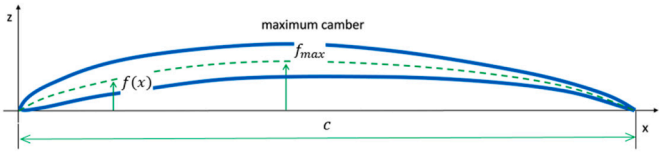


Fig. 8. Definition of camber (f(x)), maximum camber (f_{max}) and chord (c) on a generic airfoil.

Table 5
Main properties of the conducted FEM analysis.

Property	Value
Processing time (s)	30
Number of nodes	3773
Number of elements	10,881
Geometrical model	Blended curvature-based mesh
Element type	Tetrahedral solid elements with 4 Jacobian points
Maximum element size (mm)	5.43
Minimum element size (mm)	1.09

It should be noted that the increase in maximum camber is practically only due to the camber increase of the lower surface, whereas the upper surface suffers slight deformations even close to the root. This behavior can be observed in both composite structures.

Fig. 11 shows the resulting dimensionless maximum camber along the wingspan. Five different configurations are represented, corresponding to layout a, b and c and carbon (C) or glass (G) fiber. The original maximum camber value of the E61 airfoil is also represented to serve as a reference.

Cases a and b offer positive results, since all configurations produce a significant increment in camber. Two conclusions are immediate: glass fiber produces a more remarkable deformation, thanks to its significantly lower value of elastic modulus (25 against 70 GPa), and the 57 mm wide actuator produces a more important response than the 28 mm one. However, the effect of using a wider actuator is not as strong as expected, as the relative increment in camber is far from the results a linear extrapolation of the 28 mm results would predict. Besides, the overall increments derived from using a wider actuator are similar in absolute value when analyzing carbon and glass fiber composites. Notwithstanding, taking into account the higher variation produced in the glass fiber model, it can be inferred that the increment in width is relatively more efficient in the carbon fiber case.

On the other hand, configuration c proves to be inadequate, as along two thirds of the wingspan the value of maximum camber decreases with respect to that of the original airfoil. This will probably be caused by the interaction between the deformation mechanisms originated by each actuator.

Finally, Fig. 12 represents the increment in the wingtip z coordinate along the chord for configuration d. As mentioned above, it is sought to achieve a higher dihedral angle to render the aircraft more stable. Besides, a higher dihedral angle has a positive influence in reducing the wingtip-vortex-induced drag in a manner similar to conventional winglets [30]. Four different variations are considered: glass (G-) and carbon (C-) fiber and actuators located on the lower (-L) and upper (-U) skin.

Locating the actuators on the lower surface leads to a positive effect along almost all the chord. Moreover, the glass fiber model experiences a deformation mechanism parallel to the carbon fiber model, but at a more noticeable scale. In addition, the carbon and upper surface configuration clearly outstands the others as the best option to achieve a higher dihedral angle.

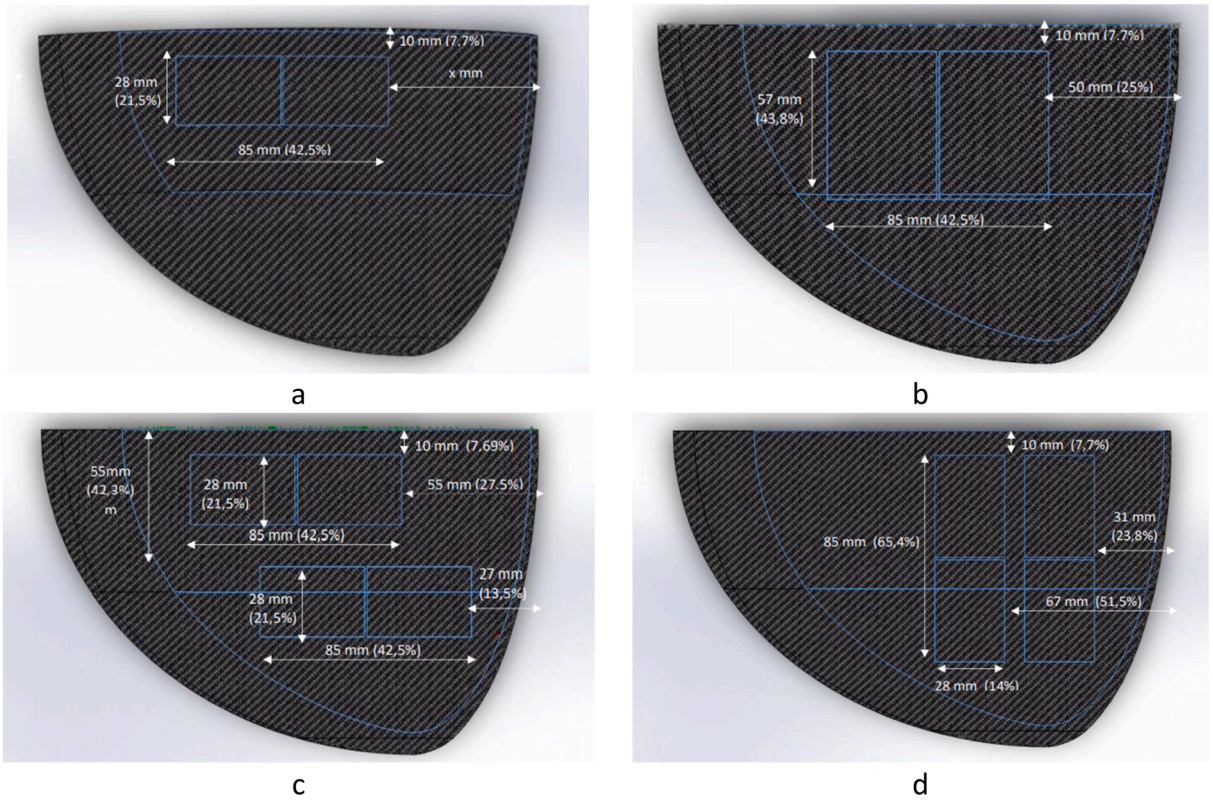


Fig. 9. Studied configurations.

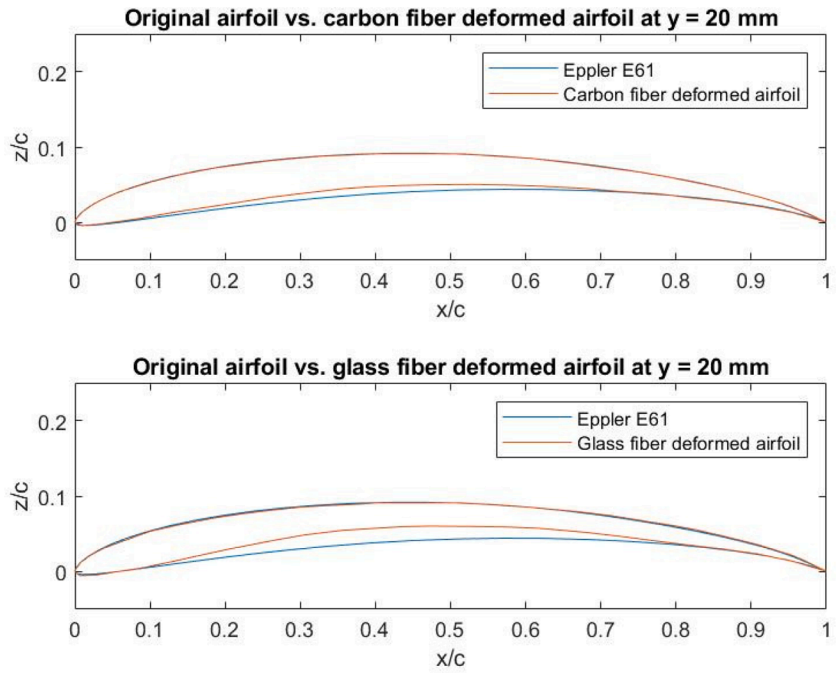


Fig. 10. Deformed airfoils at position along the wingspan y = 20 mm compared to the original E61 airfoil. Upper plot corresponds to carbon fiber composite. Lower plot corresponds to glass fiber composite.

7. Experimental aerodynamics coefficients

So as to validate the adequateness of the aforementioned geometry variations as an effective way to improve the MAV's performance, an extensive campaign of test experiments to obtain the aerodynamics coefficients of the MAV in its base configuration and its maximum deformation configuration has been carried out. The experiments have been performed in the Low-Speed Wind Tunnel of INTA, which is a closed-circuit tunnel with an elliptical test section of $2 \times 3\ m^2$. A balance with an XFC300 load cell has been used to obtain drag force of the MAV model, while Particle Image Velocimetry (PIV) has been used to measure lift force. The MAV model was placed on the wind tunnel floor by means

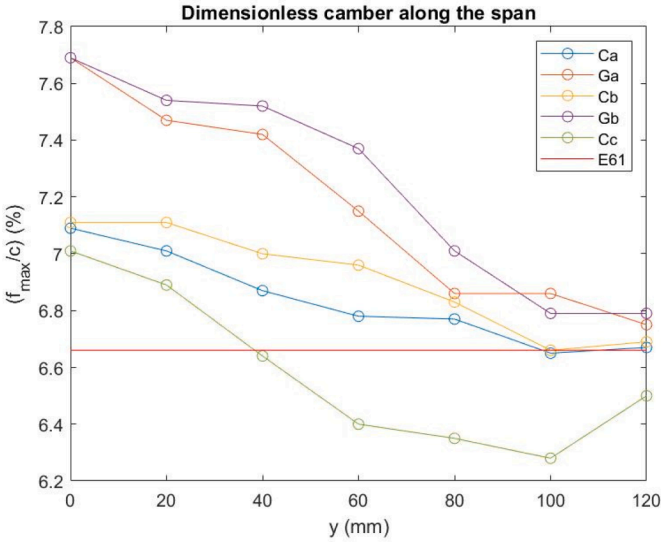


Fig. 11. Dimensionless camber along the span (layouts a, b and c).

of a streamlined support strut in order to reduce possible flow perturbations.

The prototype has been manufactured in full-scale with a low-cost 3D printing machine to give a quick response in the experimental campaign, reducing manufacturing time and cost. The additive material used is PLA (Polylactic Acid), a common thermoplastic used in wind tunnel testing. The MAV model has been tested for a wide flight range, from cruise condition (angle of attack $\alpha = 0^{\circ}$) to complete stall condition ($\alpha = 30^{\circ}$). The air velocity of the wind tunnel was 10 m/s, which lead to a Reynolds number (R_e) of 1.30×10^5, within the normal operating range for this type of vehicle. The sideslip is zero degrees. Lift (C_L) and drag (C_D) coefficients are calculated by applying the following equations:

$$C_L = \frac{L}{\frac{1}{2}\rho {U_\infty}^2 S_{ref}} C_D = \frac{D}{\frac{1}{2}\rho {U_\infty}^2 S_{ref}}$$

where ρ is air density ($\rho = 1.225\, kg/m^3$), U_∞ is freestream velocity ($U_\infty = 10\, m/s$) and S_{ref} is wing reference area ($S_{ref} = 0.04\, m^2$).

In Fig. 13, the curves of lift and drag coefficients according to the angle of attack are plotted. Lift coefficient increases with the angle of attack for both MAV configurations until reaching its maximum value. After that, the vehicle reaches stall entry condition, where the flow is detached and lift decreases rapidly. Lift values obtained in all flight regimes are higher in the maximum deformation configuration. The maximum value of lift coefficient (C_{Lmax}) obtained with the base configuration of the MAV is 1.30 at $\alpha = 25^{\circ}$, while that value increases up to 1.50 with a higher angle of attack $\alpha = 27^{\circ}$ for the maximum deformation configuration.

If only the improvement in lift force were taken into account in the aerodynamic analysis, maximum camber configuration would be implemented in all flight segments. However, optimal flight requires optimal aerodynamic efficiency in each flight phase, which implies minimizing the quotient of lift force divided by drag force. The data obtained from the balance measurements show an increase in total drag with the maximum wing deformation configuration for all angles of attack. The base configuration of the MAV should be deployed in cruise flight as the MAV generates the same lift at $\alpha = 0^{\circ}$ with a lower total drag. However, in landing and take-off maneuvers, as well as in missions requiring a lower flight speed to adapt to the payload requisites, the configuration of maximum wing deformation should be used since lift is higher and stall condition is delayed.

8. Conclusions

A bioinspired MAV prototype has been designed in order to perform an in-depth study of the deformation mechanisms induced by attaching MFC actuators to the wing surface and to verify the feasibility of using this technology to enhance its performance. Experimental tests on a half-wing model have resulted in an increment in camber when a positive voltage is applied, and a well-fitting linear function relating maximum camber to voltage has been obtained. Besides, it has been found that the leading and trailing edge boundary conditions determine a negligible increment in chord, which is considered positive for the further structural design of the aircraft.

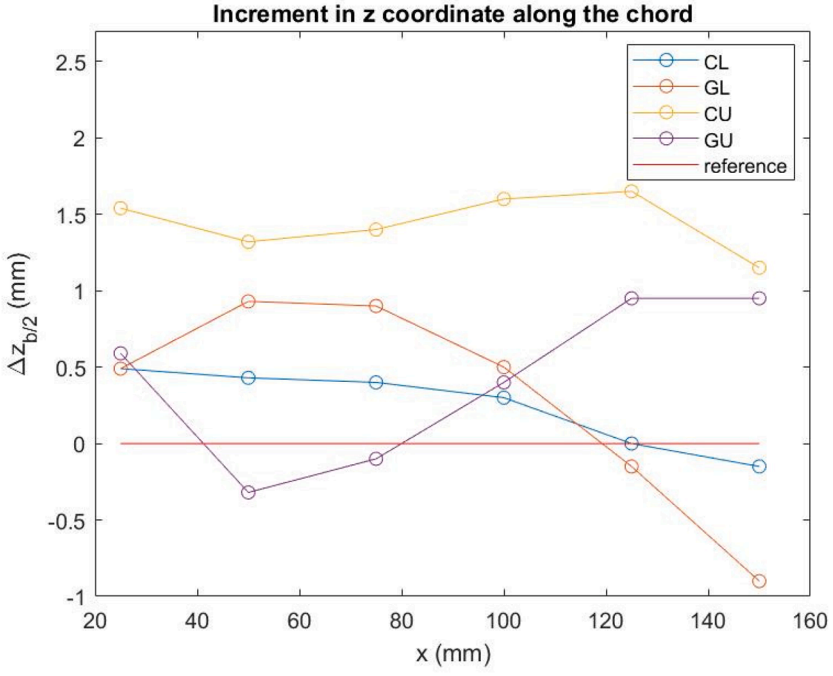


Fig. 12. Increment in wingtip z coordinate along the chord (layout d).

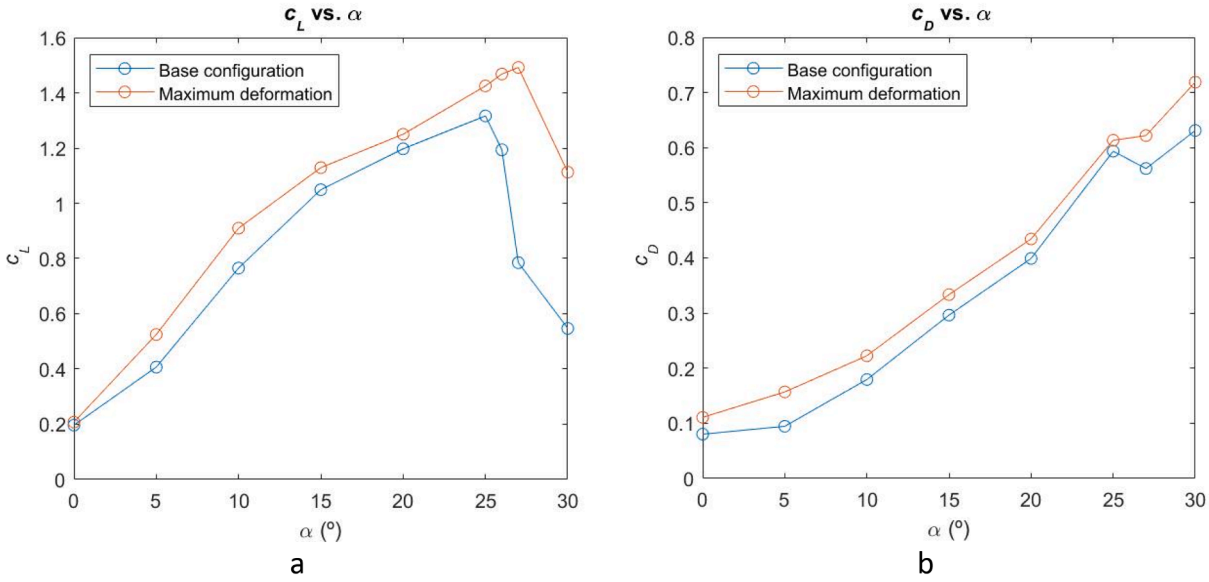


Fig. 13. Lift coefficient (a) and drag coefficient (b) vs. angle of attack for base configuration (Eppler 61 airfoil) and maximum deformation configuration (deformed Eppler 61 airfoil).

On the other hand, a thorough finite element analysis on different configurations has been performed using SOLIDWORKS®, in order to analyze the influence of different variables. The effect of the actuator position, size and number, as well as the structure material, has been studied. It has been stated that using a single actuator in each half-wing is preferable to using two, since when two actuators are used, the deformation mechanisms induced by each of them interact and produce a decrement in camber. Glass fiber composite produces a higher deformation than carbon fiber composite, thanks to its lower value of elastic modulus. Therefore, the use of MFC actuators would be more effective in aircraft manufacturing using the former material. In addition, using a 57 mm wide actuator slightly improves the results of the 28 mm wide one. However, the relative increment in camber is lower than expected considering the relative increment in actuator width.

Finally, an increment in dihedral angle has been sought in the finite element analysis, as this would cause a betterment in stability. To do that, two actuators aligned spanwise have been simulated. Four different configurations have been studied, corresponding to glass and carbon fiber composite and actuators placed on the lower and upper surface. Actuators located on the lower surface have a moderate positive effect, with the glass fiber configuration showing the same tendency as the carbon fiber, yet in a more pronounced scale. Furthermore, the best configuration to achieve this objective has proven to be the use of two actuators attached to the carbon fiber upper surface.

CRediT authorship contribution statement

Javier Crespo Moreno: Data curation, Writing – original draft, Supervision. **Rafael Bardera Mora:** Conceptualization, Methodology, Investigation, Writing – review & editing, Project administration. **Ángel Antonio Rodríguez Sevillano:** Conceptualization, Methodology, Software, Writing – review & editing. **Álvaro Cobo González:** Data curation, Writing – original draft, Visualization, Writing – review & editing.

Declaration of Competing Interest

The authors declare that they have no known competing financial interests or personal relationships that could have appeared to influence the work reported in this paper.

Data availability

The raw/processed data required to reproduce these findings cannot be shared at this time as the data also forms part of an ongoing study.

Acknowledgements

The authors would like to thank the help provided by Aeronaves y Vehículos Espaciales and Sistemas Aeroespaciales, Transporte Aéreo y Aeropuertos departments in Universidad Politécnica de Madrid, and Área de Aerodinámica Experimental in Instituto Nacional de Técnica Aeroespacial for the development of this work.

References

[1] McMichael JM, Francis MS. Micro air vehicles-toward a new dimension in flight. DARPA: Arlington, VA, United States; 1997.
[2] Wilkie W, Bryant R, High J, Fox R, Hellbaum R, Jalink Jr. A, Little B, Mirick P, Jacobs J, Low-cost piezocomposite actuator for structural control applications. In: Smart structures and materials 2000: industrial and commercial applications of smart structures technologies, proceedings of the SPIE'S 7th annual international symposium on smart structures and materials, Newport Beach, CA, United States; 6–9 March 2000. <http://doi.org/10.1117/12.388175>.
[3] Ohanian OJ, Hickling C, Stiltner B, Karni ED, Kochersberger KB, Probst T, et al. Piezoelectric morphing versus servo-actuated MAV control surfaces. In: 53rd AIAA/ASME/ASCE/AHS/ASC structures, structural dynamics and materials conference, Honolulu, HI, United States; 23–26 April 2012. doi: 10.2514/6.2012-1512.
[4] Gomez JC, Garcia E. Morphing unmanned aerial vehicles. Smart Mater Struct 2011; 20(10):103001. https://doi.org/10.1088/0964-1726/20/10/103001.
[5] Coutu D, Brailovski V, Terriault P. Optimized design of an active extrados structure for an experimental morphing laminar wing. Aerosp Sci Technol 2010;14(7): 451–8. https://doi.org/10.1016/j.ast.2010.01.009.
[6] Weisshaar T. Morphing aircraft technology – new shapes for aircraft design. RTO-MP-AVT-141, Neuilly-sur-Seine, France; 2006.
[7] Klimczyk WA, Goraj ZJ. Analysis and optimization of morphing wing aerodynamics. Aircr Eng Aerosp Tec 2019;91(3):538–46. https://doi.org/10.1108/AEAT-12-2017-0289.
[8] Sofla AYN, Meguid SA, Tan KT, Yeo WK. Shape morphing of aircraft wing: status and challenges. Mater Design 2010;31:1284–92. https://doi.org/10.1016/j.matdes.2009.09.011.
[9] Kao J, Clark D, Burton S, White T, Reich G. Planform design and optimization of morphing aircraft. In AIAA Scitech 2020 Forum, Orlando, FL, United States; 6–10 January 2020. doi: 10.2514/6.2020-1393.
[10] Chen M, Liu J, Skelton RE. Design and control of tensegrity morphing airfoils. Mech Res Commun 2020;103:103480. https://doi.org/10.1016/j.mechrescom.2020.103480.
[11] Padfield GD, Lawrence B. The birth of flight control: an engineering analysis of the wright brothers' 1902 glider. Aeronaut J 2003;107(1078):697–718. https://doi.org/10.1017/S0001924000013464.

[12] Dong Y, Boming Z, Jun L. A changeable aerofoil actuated by shape memory alloy springs. Mat Sci Eng A-Struct Mater Prop Microestruct Process 2008;485:243–50. https://doi.org/10.1016/j.msea.2007.08.061.
[13] Strelec JK, Lagoudas DC, Khan MA, Yen J. Design and implementation of a shape memory alloy actuated reconfigurable airfoil. J Intel Mater Syst Struct 2003;14 (4–5):257–73. https://doi.org/10.1177/1045389X03034687.
[14] Barcala-Montejano MA, Rodríguez-Sevillano AA, Crespo-Moreno J, Bardera-Mora R, Silva-González, AJ. Optimized performance of a morphing micro air vehicle. In: 2015 International conference on unmanned aircraft systems (ICUAS), Denver, CO, United States; 9–12 June 2015. p. 794–800. doi: 10.1109/ICUAS.2015.7152363.
[15] Barcala-Montejano MA, Rodríguez-Sevillano AA, Bardera-Mora R, García-Ramírez J, de Nova-Trigueros J, Urcelay-Oca I, et al. Smart materials applied in a micro remotely piloted aircraft system with morphing wing. J Intell Mater Syst Struct 2018;29(16):3317–32. https://doi.org/10.1177/1045389X18783893.
[16] Barbarino S, Bilgen O, Ajaj RM, Friswell MI, Inman DJ. A review of morphing aircraft. J Intell Mater Syst Struct 2011;22(9):823–77. https://doi.org/10.1177/1045389X11414084.
[17] Pankonien AM, Faria CT, Inman DJ. Synergistic smart morphing aileron: experimental quasi-static performance characterization. J Intell Mater Syst Struct 2015;26(10):1179–90. https://doi.org/10.1177/1045389X14538530.
[18] Chen H, Xia H, Qiu Y, Xu Z, Ni QQ. Smart composites of piezoelectric particles and shape memory polymers for actuation and nanopositioning. Compos Sci Technol 2018;163:123–32. https://doi.org/10.1016/j.compscitech.2018.05.004.
[19] Williams RB, Park G, Inman DJ, Wilkie WK. An overview of composite actuators with piezoceramic fibers. In: Proceedings of the 20th International Modal Analysis Conference (IMAC XX), Los Angeles, CA, United States; 2002.
[20] Williams RB. Nonlinear mechanical and actuation characterization of piezoceramic fiber composites. Blacksburg, VA, United States: Virginia Polytechnic Institute and State University; 2004.
[21] Huber C, Spori DM, Melnykowycz MM, Barbezat M. Active fiber composites: optimization of the manufacturing process and their poling behavior. In: Proceedings Volume 5761, Smart Structures and Materials 2005: Active Materials: Behavior and Mechanics, San Diego, CA, United States; 7–10 March 2005. doi: 10.1117/12.599498.
[22] Medeiros R, Rodríguez-Ramos R, Guinovart-Díaz R, Bravo-Castillero J, Otero JA, Volnei T. Numerical and analytical analyses for active fiber composite piezoelectric composite materials. J Intell Mater Syst Struct 2015;26(1):101–18. https://doi.org/10.1177/1045389X14521881.
[23] Raghavan AC, Cesnik CES. Review of guided-wave structural health monitoring. The Shock and Vibration Digest 2007;39(2):91–114. https://doi.org/10.1177/0583102406075428.
[24] Giurgiutiu V. Review of smart-materials actuation solutions for aeroelastic and vibration control. J Intell Mater Syst Struct 2000;11(7):525–44. https://doi.org/10.1106/HYTV-NC7R-BCMM-W3CH.
[25] Erturk A, Vieira WGR, De Marqui Jr. C, Inman DJ. On the energy harvesting potential of piezoaeroelastic systems. Appl Phys Lett 2010;96(18):184103. doi: 10.1063/1.3427405.
[26] Smart Material Corp. [Online]. <https://www.smart-material.com/> [Accessed 30 03 2021].
[27] Park JS, Kim JH. Analytical development of single crystal Macro Fiber Composite actuators for active twist rotor blades. Smart Mater Struct 2005;14(4):745–53. https://doi.org/10.1088/0964-1726/14/4/033.
[28] Zhang SQ, Li YX, Schmidt R. Modeling and simulation of macro-fiber composite layered smart structures. Compos Struct 2015;126:89–100. https://doi.org/10.1016/j.compstruct.2015.02.051.
[29] Williams RB, Grimsley BW, Inman DJ, Wilkie WK. Manufacturing and mechanics-based characterization of Macro Fiber Composite actuators. In: ASME international mechanical engineering congress & exposition, New Orleans, LA, United States, 17–22 November 2002. doi: 10.1115/IMECE2002-39005.
[30] Williams RB, Inman DJ, Schultz MR, Hyer MW, Wilkie WK. Nonlinear tensile and shear behavior of Macro Fiber Composite actuators. J Compos Mater 2004;38(10): 855–69. https://doi.org/10.1177/0021998304040555.
[31] Deraemaeker A, Benelechi S, Benjeddou A, Preumont A. Analytical and numerical computation of homogenized properties of MFCs: application to a composite boom with MFC actuators and sensors. In: III Eccomas Thematic Conference on Smart Structures and Materials, Gdansk, Poland; 9–11 July 2007.
[32] Deraemaeker A, Nasser H, Benjeddou A, Preumont A. Mixing rules for the piezoelectric properties of Macro Fiber Composites. J Intel Mat Syst Str 2009;20 (12):1475–82. https://doi.org/10.1177/1045389X09335615.
[33] Deraemaeker A, Nasser H. Numerical evaluation of the equivalent properties of Macro Fiber Composite (MFC) transducers using periodic homogenization. Int J Solids Struct 2010;47:3272–85. https://doi.org/10.1016/j.ijsolstr.2010.08.006.
[34] Biscani F, Nasser H, Belouettar S, Carrera E. Equivalent electro-elastic properties of macro fiber composite (MFC) transducers using asymptotic expansion approach. Compos Part B-Eng 2011;42(3):444–55. https://doi.org/10.1016/j.compositesb.2010.12.009.
[35] Bowen CR, Giddings PF, Salo AIT, Kim HA. Modeling and characterization of piezoelectrically actuated bistable composites. IEEE Trans Ultrason Ferroelect Freq Control 2011;58(9):1737–50. https://doi.org/10.1109/TUFFC.2011.2011.
[36] Zhang SQ. Numerical analysis of macro-fiber composite structures. In: Nonlinear analysis of thin-walled smart structures. Singapore: Springer; 2021. p. 137–52. 10.1007.978-981-15-9857-9_7.
[37] Rao MN, Schmidt R, Schröder KU. Large deflection electro-mechanical analysis of composite structures bonded with macro-fiber composite actuators considering thermal loads. Eng Comput-Germany 2021. https://doi.org/10.1007/s00366-020-01274-7.
[38] Lee AJ, Inman DJ. Electromechanical modelling of a bistable plate with Macro Fiber Composites under nonlinear vibrations. J Sound Vibr 2019;446:326–42. https://doi.org/10.1016/j.jsv.2019.01.045.
[39] Padoin E, Santos IF, Perondi EA, Menuzzi O, Gonçalves JF. Topology optimization of piezoelectric macro-fiber composite patches on laminated plates for vibration suppression. Struct Multidiscip Optim 2019;59:941–57. https://doi.org/10.1007/s00158-018-2111-3.